Matter and Radiation at Extremes | RESEARCH ARTICLE | scitation.org/journal/mre

Pressure-induced robust emission in a zero-dimensional hybrid metal halide $(C_9NH_{20})_6Pb_3Br_{12}$

HPSTAR 1226-2021

Cite as: Matter Radiat. Extremes 6, 058401 (2021); doi: 10.1063/5.0058821
Submitted: 2 June 2021 • Accepted: 6 August 2021 •
Published Online: 25 August 2021

View Online Export Citation CrossMark

Mengting Chen,[1] Songhao Guo,[1] Kejun Bu,[1] Sujin Lee,[2] Hui Luo,[1] Yiming Wang,[1] Bingyan Liu,[1] Zhipeng Yan,[1] Hongliang Dong,[1] Wenge Yang,[1] Biwu Ma,[2] and Xujie Lü[1,a)]

AFFILIATIONS

[1]Center for High Pressure Science and Technology Advanced Research (HPSTAR), 1690 Cailun Road, Shanghai 201203, People's Republic of China
[2]Department of Chemistry and Biochemistry, Florida State University, Tallahassee, Florida 32310, USA

Note: This paper is a part of the Special Topic Collection on High Pressure Science 2021.
[a)]**Author to whom correspondence should be addressed:** xujie.lu@hpstar.ac.cn

ABSTRACT

Zero-dimensional (0D) hybrid metal halides are under intensive investigation owing to their unique physical properties, such as the broadband emission from highly localized excitons that is promising for white-emitting lighting. However, fundamental understanding of emission variations and structure–property relationships is still limited. Here, by using pressure processing, we obtain robust exciton emission in 0D $(C_9NH_{20})_6Pb_3Br_{12}$ at room temperature that can survive to 80 GPa, the recorded highest value among all the hybrid metal halides. *In situ* experimental characterization and first-principles calculations reveal that the pressure-induced emission is mainly caused by the largely suppressed phonon-assisted nonradiative pathway. Lattice compression leads to phonon hardening, which considerably weakens the exciton–phonon interaction and thus enhances the emission. The robust emission is attributed to the unique structure of separated spring-like $[Pb_3Br_{12}]^{6-}$ trimers, which leads to the outstanding stability of the optically active inorganic units. Our findings not only reveal abnormally robust emission in a 0D metal halide, but also provide new insight into the design and optimization of local structures of trimers and oligomers in low-dimensional hybrid materials.

I. INTRODUCTION

Organic–inorganic hybrid metal halides are promising materials for use in advanced optoelectronics applications owing to their unique structural and physical properties, such as soft lattices, adjustable bandgap, and high absorption coefficient.[1–3] Dimensionality engineering at molecular levels has been demonstrated to be an effective route for increasing the diversity of their architectures and improving their stability as the optically active inorganic clusters are tailored by hydrophobic cations.[4–6] Recently, low-dimensional (low-D) metal halides have drawn great interest for their outstanding properties, including broadband emission from self-trapped excitons (STEs), potential high emission efficiency, and large Stokes shift.[7,8] Especially for the zero-dimensional (0D) metal halides, near-unity photoluminescence quantum yield (PLQY) has been achieved by optimizing compositions and local structures.[9,10] Current research focuses mainly on chemical tailoring, such as cation engineering, which is limited by tunability and may introduce a variety of influencing factors.[11–13] A systematic understanding of how structure tuning affects optical properties is still lacking, and there is therefore an urgent need for the development of advanced methods for regulation and *in situ* characterization.

It is well known that exciton emission properties depend strongly on lattice and electronic characteristics, such as structural distortions of polyhedral frameworks and the exciton binding energy.[14–16] Thus, the exciton emission can be effectively modulated by controllably regulating the lattice and electronic features using chemical methods or external stimuli like temperature and pressure.[17–19] The application of pressure is an effective and clean way to tune the structures and properties of functional materials.[20–23] Using diamond anvil cells to apply high pressure, the bond distances and

structural distortions of soft low-D metal halides can be effectively adjusted and their photophysical process and optical properties can be monitored *in situ*. There has recently been an increase in the number of studies focusing on pressure-enhanced and/or induced emission in low-D metal halides, although it is known that emission will be quenched at higher pressures. So far, no system has been found that can exhibit photoluminescence (PL) at pressures above 30 GPa.[24,25] The microscopic origin of the enhancement also remains unclear.

In this work, we report pressure-induced, enhanced, and robust emission up to 80 GPa in a 0D hybrid metal halide $(C_9NH_{20})_6Pb_3Br_{12}$, hereinafter referred to as $(bmpy)_6[Pb_3Br_{12}]$ (where bmpy = 1-butyl-1-methylpyrrolidinium), which possesses linear $[Pb_3Br_{12}]^{6-}$ trimer clusters (face-sharing octahedra) isolated by organic cations.[13,26] Using pressure regulation in combination with *in situ* structural and optical characterization, we have systematically investigated pressure-dependent photophysical properties. The pressure-induced emission (PIE) is attributed to the largely suppressed phonon-assisted non-radiative pathway. The exciton–phonon interaction is considerably reduced owing to the phonon hardening that occurs upon compression. Impressively, the emission of $(bmpy)_6[Pb_3Br_{12}]$ is still observable even at 80 GPa, which is the highest-recorded emission pressure for any kind of hybrid metal halide material. Such a robust emission is mainly due to the stiffness of the spring-like $[Pb_3Br_{12}]^{6-}$ trimers.

II. RESULTS AND DISCUSSION

To investigate the evolution of the emission properties of 0D $(bmpy)_6[Pb_3Br_{12}]$ under high pressure, *in situ* PL measurements were performed, as shown in Fig. 1. The emission is undetectable at ambient pressure, and a pressure-induced emission (PIE) centered at around 650 nm with a full width at half maximum (FWHM) of 175 nm can be observed at 1.6 GPa [inset in the left panel of Fig. 1(a)]. Such a broadband emission in this material originates from the excitons resulting from the strong electron–phonon coupling in the completely isolated individual $[Pb_3Br_{12}]^{6-}$ trimer clusters. As the pressure increases, the PL shows a remarkable enhancement and reaches a maximum at around 26 GPa. Upon further compression, the PL intensity gradually decreases with further compression [Fig. 1(a), right panel]. Figure 1(b) shows the integrated PL intensity of $(bmpy)_6[Pb_3Br_{12}]$ as a function of pressure. Strikingly, the emission can still be detected even at 80 GPa [inset in the right panel of Fig. 1(a)], a record pressure for emission in hybrid metal halides, indicating the extraordinary structural stability of this hybrid system. Such an unusually robust emission is likely due to the unique trimer clusters of this 0D metal halide, which we will elaborate on later. Besides, the fluorescence micrographs in Fig. 1(c) and in Fig. S1 in the supplementary material clearly reveal pressure-induced PL variations.

Ultraviolet–visible (UV-vis) absorption spectroscopy was utilized to elucidate the bandgap evolution of $(bmpy)_6[Pb_3Br_{12}]$ under high pressure [Fig. 2(a) and Fig. S2 in the supplementary material]. At ambient pressure, a sharp absorption edge can be found at around 350 nm upon UV irradiation. During compression, the absorption edge exhibits a continuous red shift up to 80 GPa. The bandgap evolution of $(bmpy)_6[Pb_3Br_{12}]$ is presented in Fig. 2(b), from which it can be seen that the bandgap narrows from its initial value of 3.55–2.56 eV at 80 GPa. Density functional theory (DFT) calculations of electronic structures confirm the highly localized electronic states of isolated $[Pb_3Br_{12}]^{6-}$ trimer clusters and the pressure-induced bandgap narrowing (Fig. S3 in the supplementary material) due to the increased overlapping of Pb and Br electron clouds with the shortening of Pb–Br bonds.[27] The highest occupied crystal orbital is contributed by the Pb-6*s* and Br-4*p* states, while the lowest unoccupied crystal orbital consists mainly of Pb-6*p* and Br-4*p* states.[28] By linearly fitting the pressure-dependent bandgaps, the bandgap can be tuned by less than 12.1 meV/GPa, which is lower than for the reported 0D metal halides as well as typical 3D, 2D, and 1D compounds [Fig. 2(c)], indicating a less compressible nature of the optically active inorganic unit. Optical micrographs show the color changes of the sample during compression [inset in Fig. 2(b) and Fig. S4 in the supplementary material].

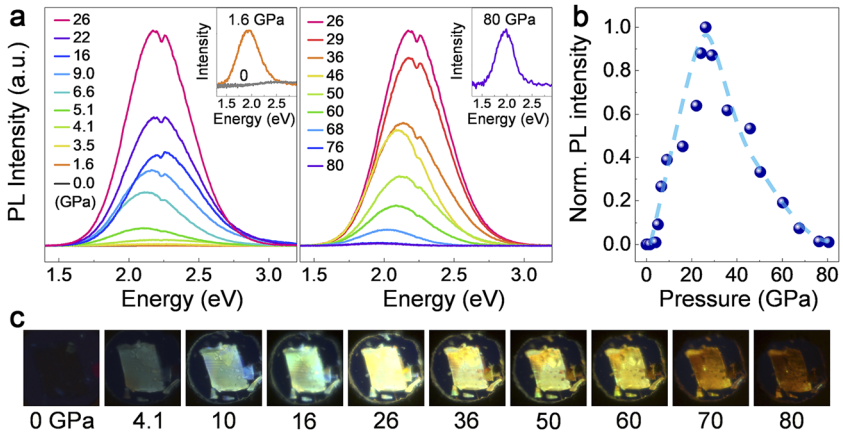

FIG. 1. *In situ* emission measurements of $(bmpy)_6[Pb_3Br_{12}]$ under high pressure. (a) PL spectra at selected pressures. The insets show the pressure-induced emission at 1.6 GPa and the robust emission at 80 GPa. The small kinks at around 2.25 eV are caused by the dichroic beam splitter (FF376-Di01, Semrock) in our measurement system. (b) Integrated PL intensity as a function of pressure. (c) Fluorescent images at selected pressures.

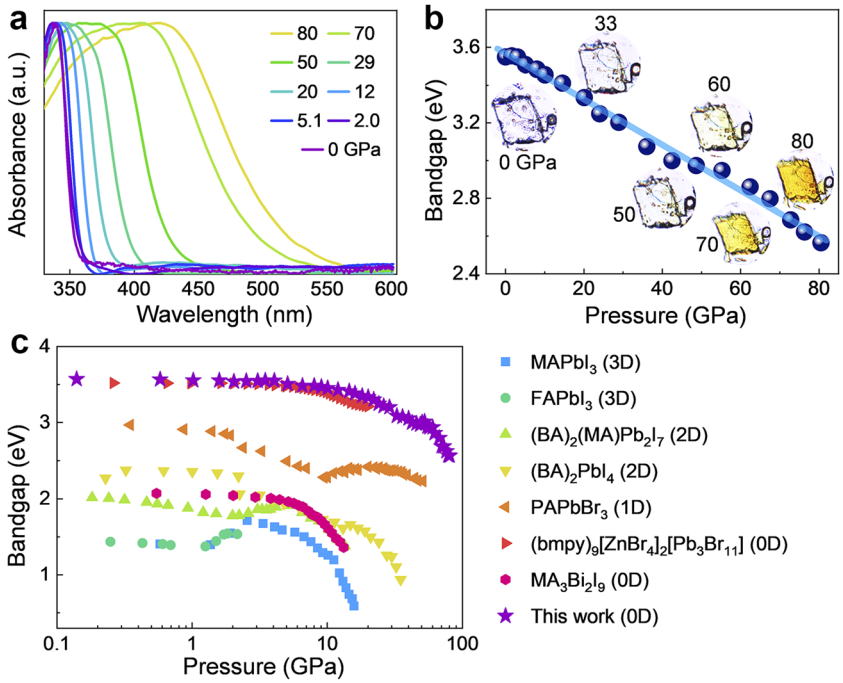

FIG. 2. Bandgap evolution of $(bmpy)_6[Pb_3Br_{12}]$ under high pressure. (a) UV-vis absorption spectra at high pressures. (b) Bandgap as a function of pressure. The insets show optical micrographs at selected pressures. (c) Bandgap evolution of $(bmpy)_6[Pb_3Br_{12}]$ compared with other hybrid metal halides, where the data are collected from the literature.[29–36]

To better understand the pressure-induced, enhanced, and robust emission of this material, *in situ* x-ray diffraction (XRD) measurements were performed up to 80 GPa. Under ambient conditions, $(bmpy)_6[Pb_3Br_{12}]$ crystallizes in a trigonal structure with space group $R\bar{3}$ and unit cell parameters $a = 17.31$ Å and $c = 22.51$ Å.[26] The $[Pb_3Br_{12}]^{6-}$ oligomers are composed of three face-sharing $[PbBr_6]^{4-}$ octahedra, and the adjacent inorganic clusters are completely isolated from each other by the surrounding large hydrophobic *N*-alkylpyrrolium cations [Fig. 3(a)]. XRD patterns at selected pressures are shown in Fig. 3(b) and in Fig. S5 in the supplementary material, where all Bragg diffraction peaks shift to higher two-theta angle with increasing pressure owing to the lattice contraction. Impressively, two main diffraction peaks, which belong to the (−1,1,1) and (−1,2,0) planes, can still be observed even at 80 GPa. No amorphization is found at

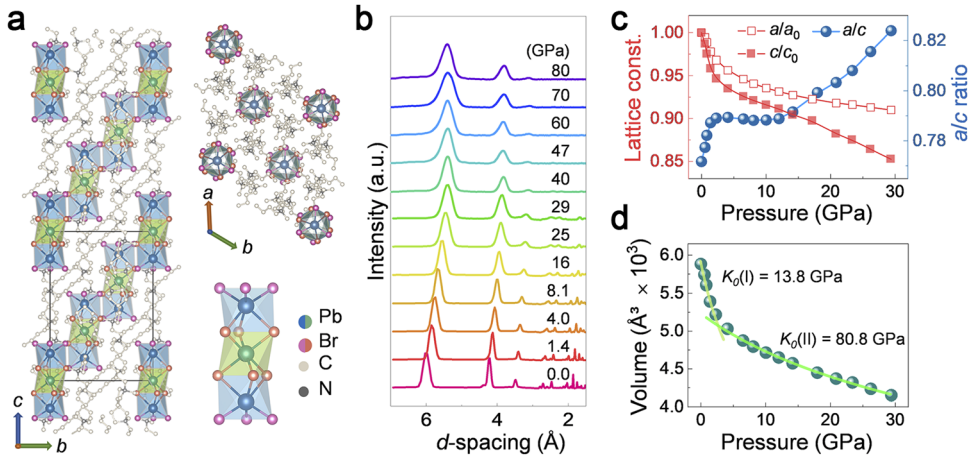

FIG. 3. *In situ* structural characterizations of $(bmpy)_6[Pb_3Br_{12}]$ under high pressure. (a) Schematic crystal structure of $(bmpy)_6[Pb_3Br_{12}]$ along different crystallographic axes and the $[Pb_3Br_{12}]^{6-}$ trimer cluster. (b) XRD patterns at selected pressures. (c) Lattice constants and *a*/*c* ratio as a function of pressure. (d) Evolution of unit-cell volumes.

such high pressures, indicating an extremely tough structure with low compressibility of the trimer clusters.

The crystal structures under high pressure were refined using the Rietveld method (Fig. S6 in the supplementary material).[37] The variations of the lattice constants are shown in Fig. 3(c) and in Table S1 in the supplementary material, and they indicate anisotropic compressibility and three-step variation during compression. With increasing pressure, the *a*/*c* ratio increases rapidly below 2 GPa, which is caused by the highly compressible organic parts and the relatively low packing factor along the *c* axis. Further increases in pressure induce an identical compression owing to the similar compressibility of the organic cations and the Pb–Br oligomers between 2 and 12 GPa. Above that, the *a*/*c* ratio continues to increase because of the different compressibilities of the octahedra along the stacking direction and those perpendicular to it. Using the Birch–Murnaghan equation of state (EoS), the pressure-dependent unit-cell volume yields bulk moduli K_0 of 13.8 and 80.8 GPa for the low- and high-pressure ranges, respectively [Fig. 3(d)].[38] Such a high bulk modulus is unusual compared with the reported values for high-pressure phases of other metal halides, such as the 0D hybrid $(bmpy)_9[ZnBr_4]_2[Pb_3Br_{11}]$ (25 GPa) and the 1D inorganic $CsCu_2I_3$ (63 GPa).[35,39] The relatively high stiffness of $(bmpy)_6[Pb_3Br_{12}]$ at high pressure is presumably due to the mechanical spring-like behavior of the $[Pb_3Br_{12}]^{6-}$ trimers, which is similar to what occurs for nanohelices and the pTPE-AN dimer with antiparallel π–π stacking.[40,41] The claw-shaped spring frames play a role of buffering and damping, suppressing excessive deformation of the $[Pb_3Br_{12}]^{6-}$ clusters and stabilize the inorganic units.

To the best of our knowledge, almost all the hybrid metal halides possess soft lattices, which impart a highly compressible structure whether they are 3D, 2D, 1D, or 0D in nature. When the pressure exceeds a certain threshold, the structure can no longer hold, resulting in amorphization. The emission will quench during crystalline structural damage. To date, no emission from these materials can survive above 30 GPa. As is summarized in Fig. 4(a) and Table I, the PL quenching pressure value of $(bmpy)_6[Pb_3Br_{12}]$ is as high as 80 GPa, far higher than that of any other low-D metal halide.[14,24,35,39,42,43] Such a robust PL of $(bmpy)_6[Pb_3Br_{12}]$ could be attributable to its relatively high structural stability discussed above.

To obtain the local bonding information under high pressure, *in situ* Raman spectra were collected, as shown in Fig. S7 in the supplementary material. Under ambient conditions, a Raman-active mode at around 129.4 cm^{-1} can be observed, which is associated with the symmetric stretching vibration of Pb–Br bonds. With increasing pressure, the right shift of the Raman peak indicates hardening of the phonon modes. We calculated the corresponding phonon energy as a function of pressure [Fig. 4(b)], which shows a continuous increase upon compression, suggesting reduced exciton–phonon coupling.[46,55]

The strong exciton–phonon coupling gives rise to localized excitons and leads to the broadband emission in low-D metal halides. However, an overly strong exciton–phonon coupling would lead to overlap between

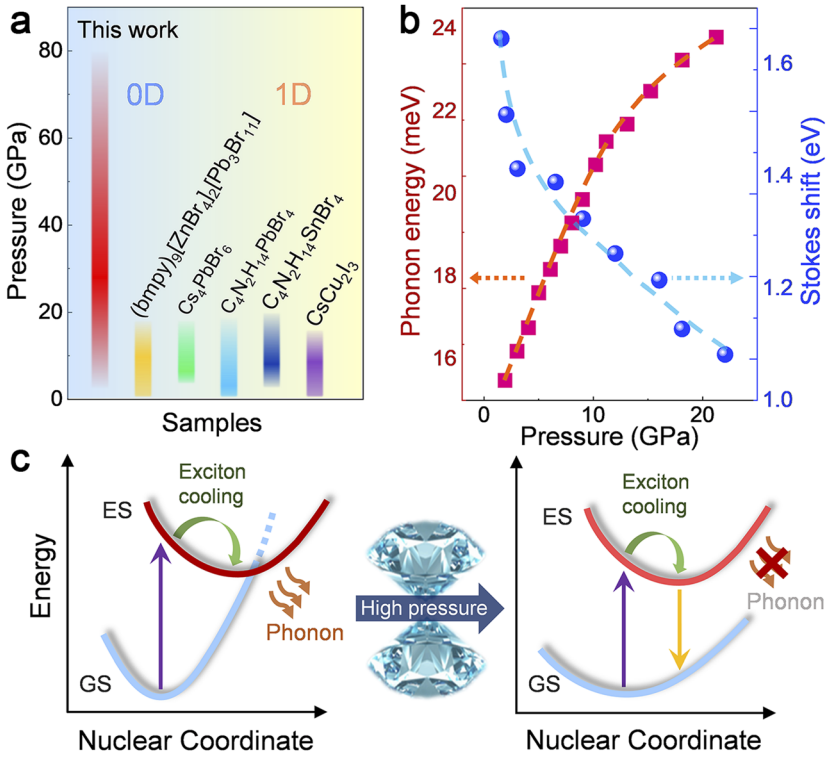

FIG. 4. (a) PL emerging and quenching pressures of $(bmpy)_6[Pb_3Br_{12}]$ in comparison with those of other 0D and 1D metal halides. (b) Stokes shift and phonon energy as functions of pressure. (c) Schematic of pressure-induced emission from excitons. GS and ES indicate the ground state and excited state, respectively.

TABLE I. Summary of PL emerging and quenching pressures for various metal halides.

Chemical formula	Dimension	PIE pressure (GPa)	PL quenching pressure (GPa)	Reference
$(bmpy)_9[ZnBr_4]_2[Pb_3Br_{11}]$	0D	Ambient	18.2	35
$(CH_3NH_3)_3Bi_2I_9$	0D	Ambient	9.0	36
Cs_4PbBr_6	0D	3.01	18.23	14
$Cs_3Bi_2I_9$	0D	Ambient	9.3	44
$C_4N_2H_{14}PbBr_4$	1D	Ambient	9.0	42
$C_4N_2H_{14}PbBr_4$	1D	Ambient	24.81	43
$C_4N_2H_{14}SnBr_4$	1D	2.06	20.02	24
$CH_3(CH_2)_2NH_3PbBr_3$	1D	Ambient	7.3	34
$CsCu_2I_3$	1D	Ambient	16.0	39
$(BA)_2PbI_4$	2D	Ambient	10	45
$(BA)_2PbI_4$	2D	Ambient	12.6	32
$(PEA)_2PbBr_4$	2D	Ambient	15.6	46
$(PEA)_2PbI_4$	2D	Ambient	7.6	47
$(HA)_2(GA)Pb_2I_7$	2D	Ambient	9.48	25
$(BA)_2(MA)Pb_2I_7$	2D	Ambient	4.7	31
$(GA)(MA)_2Pb_2I_7$	2D	Ambient	7.0	48
$(BA)_4AgBiBr_8$	2D	2.5	25.0	49
$(CH_3NH_3)PbCl_3$	3D	Ambient	7.2	50
$(CH_3NH_3)PbBr_3$	3D	Ambient	4.85	50
$(CH_3NH_3)PbBr_3$	3D	Ambient	4.0	51
$(CH_3NH_3)PbI$	3D	Ambient	2.7	52
$(CH_3NH_3)PbI_{1.2}Br_{1.8}$	3D	Ambient	1.6	53
$CsPb_2Br_5$	3D	Ambient	2.23	54
$Cs_2AgBiCl_6$	3D	Ambient	8.0	55

the excited-state (ES) curve and the ground-state (GS) one, resulting in phonon-assisted nonradiative recombination of the excited electrons and holes.[15] As has been reported, a relatively large Stokes shift exists in the low-D metal halides with face-sharing octahedra compared with the edge-sharing and corner-sharing compounds.[12,13,56–58] As shown in Fig. 4(b), $(bmpy)_6[Pb_3Br_{12}]$ exhibits a large Stokes shift of 1.7 eV at 1.6 GPa, which decreases rapidly during compression. DFT calculations on electronic structures of $(bmpy)_6[Pb_3Br_{12}]$ reveal higher dispersive frontier orbitals under high pressures, which indicates reduced exciton localization (Fig. S3 in the supplementary material). The mechanism of pressure-induced emission is illustrated in Fig. 4(c). The severe structural distortion of the face-sharing frameworks brings strong exciton–phonon interaction in $(bmpy)_6[Pb_3Br_{12}]$ at ambient conditions, raises the GS energy, and thus results in crossover between the ES and the GS. Consequently, the excitons can easily annihilate by the phonon-assisted pathway, leading to a highly nonradiative energy transfer and undetectable PL under ambient conditions. Upon compression, the lattice contraction leads to phonon hardening, which considerably weakens the exciton–phonon interaction and thus reduces the wavefunction overlap between the ES and the GS. Therefore, the phonon-assisted nonradiative loss is greatly suppressed, giving rise to exciton emission under certain high pressures.

III. CONCLUSION

In summary, pressure-induced emission has been revealed in the 0D hybrid metal halide $(bmpy)_6[Pb_3Br_{12}]$, with PL emerging at around 1.6 GPa and surviving to a record high pressure of 80 GPa among all kinds of hybrid metal halides. Through comprehensive *in situ* high-pressure characterization and first-principles calculations, the pressure-induced emission has been demonstrated to be caused by suppression of the phonon-assisted nonradiative pathway. Lattice compression hardens the phonons and reduces the exciton–phonon interaction. The robust emission is attributed to the tough sublattice of optically active spring-like trimers $[Pb_3Br_{12}]^{6-}$, indicated by the low compressibility with a relatively high bulk modulus K_0 = 80.8 GPa and the slow bandgap decrease (12.1 meV/GPa). Our findings provide new insight into the design and optimization of trimers and oligomers in low-D metal halides with the aim of achieving high performance in optoelectronics applications.

SUPPLEMENTARY MATERIAL

See the supplementary material for the experimental section and supplementary figures and tables.

ACKNOWLEDGMENTS

This work was supported by the National Nature Science Foundation of China (NSFC) (Grant Nos. U1930401 and 51527801). S.L. and B.M. are grateful for support from the National Science Foundation (Grant No. DMR-1709116). Portions of this work were performed at GeoSoilEnviroCARS (The University of Chicago, Sector 13), Advanced Photon Source (APS), Argonne National Laboratory. GeoSoilEnviroCARS is supported by the National Science Foundation – Earth Sciences (Grant No. EAR-1634415) and the Department of Energy – GeoSciences (Grant No. DE-FG02-94ER14466), and

partially by COMPRES under NSF Cooperative Agreement No. EAR-1606856.

REFERENCES

[1]Y. Chen, Y. Lei, Y. Li *et al.*, "Strain engineering and epitaxial stabilization of halide perovskites," Nature **577**, 209–215 (2020).

[2]X.-K. Liu, W. Xu, S. Bai *et al.*, "Metal halide perovskites for light-emitting diodes," Nat. Mater. **20**, 10–21 (2020).

[3]M. M. Lee, J. Teuscher, T. Miyasaka *et al.*, "Efficient hybrid solar cells based on meso-superstructured organometal halide perovskites," Science **338**, 643–647 (2012).

[4]H. Tsai, W. Nie, J.-C. Blancon *et al.*, "High-efficiency two-dimensional Ruddlesden–Popper perovskite solar cells," Nature **536**, 312–317 (2016).

[5]Z. Yuan, C. Zhou, Y. Tian *et al.*, "One-dimensional organic lead halide perovskites with efficient bluish white-light emission," Nat. Commun. **8**, 14051–14057 (2017).

[6]C. Zhou, L. Xu, S. Lee *et al.*, "Recent advances in luminescent zero-dimensional organic metal halide hybrids," Adv. Opt. Mater. **2**, 2001766 (2020).

[7]Q. Fu, X. Tang, B. Huang *et al.*, "Recent progress on the long-term stability of perovskite solar cells," Adv. Sci. **5**, 1700387 (2018).

[8]C. Zhou, H. Lin, Y. Tian *et al.*, "Luminescent zero-dimensional organic metal halide hybrids with near-unity quantum efficiency," Chem. Sci. **9**, 586–593 (2018).

[9]H. Lin, C. Zhou, Y. Tian *et al.*, "Low-dimensional organometal halide perovskites," ACS Energy Lett. **3**, 54–62 (2018).

[10]M. Li and Z. Xia, "Recent progress of zero-dimensional luminescent metal halides," Chem. Soc. Rev. **50**, 2626–2662 (2021).

[11]L.-K. Gong, J.-R. Li, Z.-F. Wu *et al.*, "Enhancing the phosphorescence of hybrid metal halides through molecular sensitization," J. Mater. Chem. C **7**, 9803–9807 (2019).

[12]B. Febriansyah, C. S. D. Neo, D. Giovanni *et al.*, "Targeted synthesis of trimeric organic–bromoplumbate hybrids that display intrinsic, highly Stokes-shifted, broadband emission," Chem. Mater. **32**, 4431–4441 (2020).

[13]J. Zhou, M. Li, L. Ning *et al.*, "Broad-band emission in a zero-dimensional hybrid organic [$PbBr_6$] trimer with intrinsic vacancies," J. Phys. Chem. Lett. **10**, 1337–1341 (2019).

[14]Z. Ma, Z. Liu, S. Lu *et al.*, "Pressure-induced emission of cesium lead halide perovskite nanocrystals," Nat. Commun. **9**, 4506 (2018).

[15]S. Li, J. Luo, J. Liu *et al.*, "Self-trapped excitons in all-inorganic halide perovskites: Fundamentals, status, and potential applications," J. Phys. Chem. Lett. **10**, 1999–2007 (2019).

[16]S. Guo, K. Bu, J. Li *et al.*, "Enhanced photocurrent of all-inorganic two-dimensional perovskite $Cs_2PbI_2Cl_2$ via pressure-regulated excitonic features," J. Am. Chem. Soc. **143**, 2545–2551 (2021).

[17]M. Li, T. Liu, Y. Wang *et al.*, "Pressure responses of halide perovskites with various compositions, dimensionalities, and morphologies," Matter Radiat. Extremes **5**, 018201 (2020).

[18]C. Pei and L. Wang, "Recent progress on high-pressure and high-temperature studies of fullerenes and related materials," Matter Radiat. Extremes **4**, 028201 (2019).

[19]C. S. Yoo, "Chemistry under extreme conditions: Pressure evolution of chemical bonding and structure in dense solids," Matter Radiat. Extremes **5**, 018202, (2020).

[20]X. Lü, C. Stoumpos, Q. Hu *et al.*, "Regulating off-centering distortion maximizes photoluminescence in halide perovskites," Natl. Sci. Rev. (published online) (2020).

[21]A. Navrotsky, "Pressure-induced structural changes cause large enhancement of photoluminescence in halide perovskites: A quantitative relationship," Natl. Sci. Rev. (published online) (2021).

[22]H. K. Mao and W. L. Mao, "Key problems of the four-dimensional earth system," Matter Radiat. Extremes **5**, 038102 (2020).

[23]H. K. Mao, B. Chen, H. Gou *et al.*, "2020—Transformative science in the pressure dimension," Matter Radiat. Extremes **6**, 013001 (2020).

[24]Y. Shi, Z. Ma, D. Zhao *et al.*, "Pressure-induced emission (PIE) of one-dimensional organic tin bromide perovskites," J. Am. Chem. Soc. **141**, 6504–6508 (2019).

[25]S. Guo, Y. Zhao, K. Bu *et al.*, "Pressure-suppressed carrier trapping leads to enhanced emission in two-dimensional perovskite $(HA)_2(GA)Pb_2I_7$," Angew. Chem., Int. Ed. **59**, 17533–17539 (2020).

[26]S. Lee, C. Zhou, J. Neu *et al.*, "Bulk assemblies of lead bromide trimer clusters with geometry-dependent photophysical properties," Chem. Mater. **32**, 374–380 (2020).

[27]B. J. Foley, D. L. Marlowe, K. Sun *et al.*, "Temperature dependent energy levels of methylammonium lead iodide perovskite," Appl. Phys. Lett. **106**, 243904 (2015).

[28]J. G. Santaclara, F. Kapteijn, J. Gascon *et al.*, "Understanding metal–organic frameworks for photocatalytic solar fuel production," CrystEngComm **19**, 4118–4125 (2017).

[29]A. Jaffe, Y. Lin, W. L. Mao *et al.*, "Pressure-induced metallization of the halide perovskite $(CH_3NH_3)PbI_3$," J. Am. Chem. Soc. **139**, 4330–4333 (2017).

[30]H. Zhu, T. Cai, M. Que *et al.*, "Pressure-induced phase transformation and band-gap engineering of formamidinium lead iodide perovskite nanocrystals," J. Phys. Chem. Lett. **9**, 4199–4205 (2018).

[31]G. Liu, L. Kong, P. Guo *et al.*, "Two regimes of bandgap red shift and partial ambient retention in pressure-treated two-dimensional perovskites," ACS Energy Lett. **2**, 2518–2524 (2017).

[32]Y. Yuan, X. Liu, X. Ma *et al.*, "Large band gap narrowing and prolonged carrier lifetime of $(C_4H_9NH_3)_2PbI_4$ under high pressure," Adv. Sci. **6**, 1900240 (2019).

[33]Q. Li, Y. Wang, W. Pan *et al.*, "High-pressure band-gap engineering in lead-free $Cs_2AgBiBr_6$ double perovskite," Angew. Chem., Int. Ed. **129**, 16185–16189 (2017).

[34]X. Ren, X. Yan, A. S. Ahmad *et al.*, "Pressure-induced phase transition and band gap engineering in propylammonium lead bromide perovskite," J. Phys. Chem. C **123**, 15204–15208 (2019).

[35]Q. Li, Z. Chen, M. Li *et al.*, "Pressure-engineered photoluminescence tuning in zero-dimensional lead bromide trimer clusters," Angew. Chem., Int. Ed. **60**, 2583–2587 (2020).

[36]L. Zhang, C. Liu, Y. Lin *et al.*, "Tuning optical and electronic properties in low-toxicity organic–inorganic hybrid $(CH_3NH_3)_3Bi_2I_9$ under high pressure," J. Phys. Chem. Lett. **10**, 1676–1683 (2019).

[37]H. M. Rietveld, "A profile refinement method for nuclear and magnetic structures," J. Appl. Crystallogr. **2**, 65–71 (1969).

[38]F. Birch, "Finite elastic strain of cubic crystals," Phys. Rev. **71**, 809–824 (1947).

[39]Q. Li, Z. Chen, B. Yang *et al.*, "Pressure-induced remarkable enhancement of self-trapped exciton emission in one-dimensional $CsCu_2I_3$ with tetrahedral units," J. Am. Chem. Soc. **142**, 1786–1791 (2020).

[40]H. Liu, Y. Gu, Y. Dai *et al.*, "Pressure-induced blue-shifted and enhanced emission: A cooperative effect between aggregation-induced emission and energy-transfer suppression," J. Am. Chem. Soc. **142**, 1153–1158 (2020).

[41]D. C. Hooper, A. G. Mark, C. Kuppe *et al.*, "Strong rotational anisotropies affect nonlinear chiral metamaterials," Adv. Mater. **29**, 1605110 (2017).

[42]Y. Wang, S. Guo, H. Luo *et al.*, "Reaching 90% photoluminescence quantum yield in one-dimensional metal halide $C_4N_2H_{14}PbBr_4$ by pressure-suppressed nonradiative loss," J. Am. Chem. Soc. **142**, 16001–16006 (2020).

[43]Z. Ma, F. Li, L. Sui *et al.*, "Tunable color temperatures and emission enhancement in 1D halide perovskites under high pressure," Adv. Opt. Mater. **8**, 2000713 (2020).

[44]L. Zhang, C. Liu, L. Wang *et al.*, "Pressure-induced emission enhancement, band-gap narrowing, and metallization of halide perovskite $Cs_3Bi_2I_9$," Angew. Chem., Int. Ed. **57**, 11213–11217 (2018).

[45]T. Yin, B. Liu, J. Yan *et al.*, "Pressure-engineered structural and optical properties of two-dimensional $(C_4H_9NH_3)_2PbI_4$ perovskite exfoliated nm-thin flakes," J. Am. Chem. Soc. **141**, 1235–1241 (2019).

[46]L. Zhang, L. Wu, K. Wang *et al.*, "Pressure-induced broadband emission of 2D organic–inorganic hybrid perovskite," Adv. Sci. **6**, 1801628 (2019).

[47]S. Liu, S. Sun, C. K. Gan *et al.*, "Manipulating efficient light emission in two-dimensional perovskite crystals by pressure-induced anisotropic deformation," Sci. Adv. **5**, eaav9445 (2019).

[48]Y. Chen, R. Fu, L. Wang *et al.*, "Emission enhancement and bandgap retention of a two-dimensional mixed cation lead halide perovskite under high pressure," J. Mater. Chem. A **7**, 6357–6362 (2019).

[49]Y. Fang, L. Zhang, L. Wu *et al.*, "Pressure-induced emission (PIE) and phase transition of a two-dimensional halide double perovskite $(BA)_4AgBiBr_8$ ($BA=CH_3(CH_2)_3NH_3^+$)," Angew. Chem., Int. Ed. **58**, 15249 (2019).

[50]K. Matsuishi, T. Ishihara, S. Onari *et al.*, "Optical properties and structural phase transitions of lead-halide based inorganic–organic 3D and 2D perovskite semiconductors under high pressure," Phys. Status Solidi B **241**, 3328–3333 (2004).

[51]T. Yin, Y. Fang, W. K. Chong *et al.*, "High-pressure-induced comminution and recrystallization of $CH_3NH_3PbBr_3$ nanocrystals as large thin nanoplates," Adv. Mater. **30**, 1705017 (2018).

[52]S. Jiang, Y. Fang, R. Li *et al.*, "Pressure-dependent polymorphism and band-gap tuning of methylammonium lead iodide perovskite," Angew. Chem., Int. Ed. **55**, 6540–6544 (2016).

[53]A. Jaffe, Y. Lin, C. M. Beavers *et al.*, "High-pressure single-crystal structures of 3D lead-halide hybrid perovskites and pressure effects on their electronic and optical properties," ACS Cent. Sci. **2**, 201–209 (2016).

[54]Z. Ma, F. Li, G. Qi *et al.*, "Structural stability and optical properties of two-dimensional perovskite-like $CsPb_2Br_5$ microplates in response to pressure," Nanoscale **11**, 820–825 (2019).

[55]L. Zhang, Y. Fang, L. Sui *et al.*, "Tuning emission and electron–phonon coupling in lead-free halide double perovskite $Cs_2AgBiCl_6$ under pressure," ACS Energy Lett. **4**, 2975–2982 (2019).

[56]M. E. Kamminga, H.-H. Fang, M. R. Filip *et al.*, "Confinement effects in low-dimensional lead iodide perovskite hybrids," Chem. Mater. **28**, 4554–4562 (2016).

[57]C. Zhou, H. Lin, M. Worku *et al.*, "Blue emitting single crystalline assembly of metal halide clusters," J. Am. Chem. Soc. **140**, 13181–13184 (2018).

[58]J. M. Hoffman, X. Che, S. Sidhik *et al.*, "From 2D to 1D electronic dimensionality in halide perovskites with stepped and flat layers using propylammonium as a spacer," J. Am. Chem. Soc. **141**, 10661–10676 (2019).